Journal of Electrochemistry

Volume 23
Issue 2 *Special Issue in Honor of Professor Zhaowu Tian on His 90th Birthday*

2017-04-28

Electrodeposition of RuO_2 Layers on TiO_2 Nanotube Array toward CO_2 Electroreduction

Bei Jiang

Lina Zhang

Xianxian Qin

Wenbin Cai
Shanghai Key Laboratory of Molecular Catalysis and Innovative Materials, Collaborative Innovation Center of Chemistry for Energy Materials, Department of Chemistry, Fudan University, Shanghai 200433, China;, wbcai@fudan.edu.cn

Recommended Citation

Bei Jiang, Lina Zhang, Xianxian Qin, Wenbin Cai. Electrodeposition of RuO_2 Layers on TiO_2 Nanotube Array toward CO_2 Electroreduction[J]. *Journal of Electrochemistry*, 2017 , 23(2): 238-244.
DOI: 10.13208/j.electrochem.161253
Available at: https://jelectrochem.xmu.edu.cn/journal/vol23/iss2/13

DOI: 10.13208/j.electrochem.161253 **Artical ID**:1006-3471(2017)02-0238-07
Cite this: *J. Electrochem.* **2017**, *23*(2): 238-244 **Http**://electrochem.xmu.edu.cn

Electrodeposition of RuO_2 Layers on TiO_2 Nanotube Array toward CO_2 Electroreduction

Bei Jiang, Lina Zhang, Xianxian Qin, Wenbin Cai*

(*Shanghai Key Laboratory of Molecular Catalysis and Innovative Materials, Collaborative Innovation Center of Chemistry for Energy Materials, Department of Chemistry, Fudan University, Shanghai* 200433, *China*)

Abstract: RuO_2/TiO_2 composite materials have multitude of electrocatalytic applications including but not limited to CO_2 reduction reaction (CO_2RR). RuO_2/TiO_2 electrodes were previously prepared by repetitive coating and thermal decomposition (TD) of a Ru(III) precursor solution on Ti substrate. In this work, electrochemical potential cycling is applied to deposit amorphous RuO_2 (α-RuO_2) layers onto TiO_2 nanotube array (TNA) (RuO_2^{CV}/TNA) preformed on Ti foil. SEM, GIXRD, and voltammetry are applied to characterize the structures of the resulting RuO_2^{CV}/TNA. Ru loading on the RuO_2^{CV}/TNA electrode is *ca.* 1/30 of that on the conventional RuO_2^{TD}/TNA electrode. Although both electrodes yield similar faradaic efficiencies (FEs) for the reduction products, the RuO_2^{CV}/TNA electrode displays a much higher reduction current, a more positive initial reduction potential and a better durability than the RuO_2^{TD}/TNA one. In addition to higher FEs for formate and CH_4, the RuO_2^{CV}/TNA electrode yields the product of CO for the CO_2RR in 0.1 mol·L^{-1} $KHCO_3$, which is not available in a PBS solution with pH 7.

Key words: CO_2 reduction; amorphous RuO_2; TiO_2 nanotube array; electrodeposition

CLC Number: O646 **Document Code**: A

CO_2 reduction reaction (CO_2RR) is receiving much attention[1-6] in considering that it may be used to convert the largest carbon resource in the atmosphere to value-added chemicals and in the meantime to reduce the greenhouse effect. CO_2RR may be accomplished by means of chemical hydrogenation[1], photochemical reduction[3,7-8] and electrochemical reduction[4]. Due to harsh conditions with chemical hydrogenation and very low efficiencies with photochemical reduction, electrochemical reduction is attractive for its mild conditions and diversities in converting CO_2 to CO, formate, CH_3OH and other small organic molecules, especially when the electricity comes from renewable energy sources.

CO_2RR on various metal catalysts were widely studied[9-12]. However, the high over-potentials and the vulnerability to cationic impurities may impede the applications of metal catalysts. In fact, very negative potentials such as -1.25 to -1.8 V vs SCE (namely large absolute over-potentials) are required to effectively drive CO_2RR at most metal electrodes in CO_2-saturated 0.1 mol·L^{-1} $KHCO_3$ to maintain meaningful currents[13]. The cationic impurities in solution may significantly change the activity and selectivity of the metal electrodes. To address the above concerns, metal complexes[14] and metallic oxides[15] were examined for the catalytic materials. Specifically, the conductive RuO_2[16-22] is expected to have smaller over-potential for CO_2RR as well as hydrogen adsorption, which is essential for reducing the intermediate $CO_2^{\bullet-}$ to formate. RuO_x is unexpectedly stable even under vigorous hydrogen evolution, as a result only partial reduction to Ru ox-hydroxide occurs[22]. Along this line, additional merit of using the RuO_2 catalyst for CO_2RR lies in its tolerance to cationic impurities in solution during CO_2RR so that a much more stable reduction current may be retained.

Coating a thin layer of RuO_2 on TiO_2 substrate to form the so-called RuO_2/TiO_2 composites[17,20,22] may further enhance electrocatalytic activity and durabili-

Received: 2017-04-07, Revised: 2017-04-28 *Corresponding author, Tel: (86-21)55664050, E-mail: wbcai@fudan.edu.cn

ty of RuO_2[17] for CO_2RR. High-temperature thermal decomposition (TD) of $RuCl_3$ salt solution repeatedly drop-casted on Ti foil in ambient atmosphere was routinely adopted to prepare polycrystalline RuO_2/TiO_2 electrodes, in which the amount of RuO_2 is quite high to maintain satisfactory dispersion.

To overcome the drawbacks of the traditional TD method for preparing the RuO_2/TiO_2 (denoted as RuO_2^{TD}/TNA) electrode, in this work, the potential cycling method is extended to electrodeposit amorphous RuO_2 layers onto vertically oriented TiO_2 nanotube array (TNA) preformed on Ti foil (denoted as RuO_2^{CV}/TNA) to increase the electroactive surface area while decreasing markedly the amount of RuO_2 deposit. Preliminary analysis of CO_2RR on RuO_2^{CV}/TNA in pH 7 PBS and bicarbonate solutions are conducted, showing that formate, CO, CH_4 are detectable products with significant evolution of H_2.

1 Experimental

TNA on Ti foil was formed by means of anodization according to procedures similar to previous reports[24-28], by using a Ti foil and a Pt sheet as the anode and the cathode, respectively. Before anodization, a mechanically polished Ti foil was first etched in the solution (V_{H_2O}:V_{HNO_3}:V_{HF} = 5:4:1) for 1 min at room temperature. After being rinsed with copious amount of ultrapure water, the Ti foil was anodized with a voltage of 20 V in a solution containing 0.61 mL HF and 0.39 mL CH_3COOH at 30 ℃ for 1.5 h.

The preformed TNA was sensitized in 15 mmol·L^{-1} $SnCl_2$ + 2 mol·L^{-1} HCl for 10 min, and then activated in 5 mmol·L^{-1} $PdCl_2$ + 0.5 mol·L^{-1} HCl for 10 min prior to potential cycling to trigger the growth of first α-RuO_2 layer on TNA from -0.2 V to 1.0 V for 80 cycles at a scan rate of 50 mV·s^{-1} in the plating bath of 2 mmol·L^{-1} $RuCl_3$ and 0.10 mol·L^{-1} $NaNO_3$. After that, the electrode was annealed in a muffle furnace for 2 h at 450 ℃ to polycrystalline RuO_2/TNA (pc-RuO_2/TNA), followed by potential cycling deposition of the second layer of α-RuO_2 on pc-RuO_2/TNA under otherwise same conditions depicted in the above to form the RuO_2^{CV}/TNA electrode for CO_2RR. The annealing pretreatment before the second electrodeposition is to increase the adhesion and stability of α-RuO_2 layer during CO_2RR. A schematic diagram of preparing the RuO_2^{CV}/TNA electrode is shown in Fig. 1.

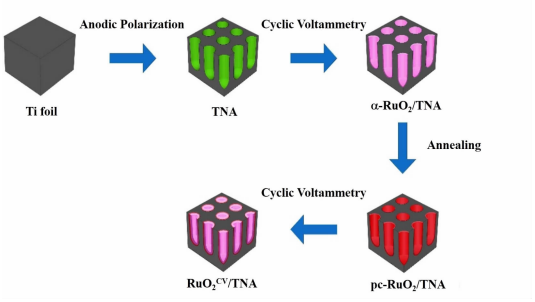

Fig. 1 Schematic illustration for preparing the RuO_2^{CV}/TNA electrode

For comparison, RuO_2^{TD}/TNA was prepared by thermal decomposition of alcoholic solution of 2 mg $RuCl_3$ on TNA (2 cm^2) in a muffle furnace for 2 h at 450 ℃. All electrochemical experiments were performed in a conventional three-compartment cell by using a Pt foil as the counter electrode and an SCE as the reference electrode, respectively. Linear sweep voltammograms and chronoamperometry curves were recorded in 0.2 mol·L^{-1} $NaClO_4$ buffered with 0.2 mol·L^{-1} Na_2HPO_4-NaH_2PO_4 (PBS, pH 7) saturated by either N_2 (99.999%) or CO_2 (99.999%). Potential dependent CO_2RR was conducted in CO_2-saturated 0.1 mol·L^{-1} $KHCO_3$ which is mostly used in literature.

The solutions were prepared with ultrapure water (Milli-Q, ⩾18.2 MΩ) and AR grade reagents as received. The surface morphologies of the samples were characterized by field emission scanning electron microscopy (FE-SEM, Hitachi S-4800), and the components were analyzed by energy dispersive X-ray spectrometry (EDX, QUANTAX 400). The crystalline structures were determined by grazing incidence X-ray diffractometry (GI-XRD, New D8 advance, Bruker) at an incident angle α_i = 0.2°. The gas products of CO_2RR were analyzed by using the GC 2060 gas chromatography while the products dissolved in the electrolyte was analyzed by NMR (500 MHz, Bruker) and IC (Dionex DX-500).

2 Results and Discussion

Fig. 2A-C show the FE-SEM images for TNA before and after deposition of RuO_2 layers. The TiO_2 nanotubes are vertically aligned with a diameter of 91 ± 15 nm and a wall thickness of 13 ± 3 nm (Fig. 2A). After the first deposition of α-RuO_2 on TNA, the nanotube wall thickness increases to 17 ± 4 nm, and it further increases to 30 ± 5 nm after the second potential cycling deposition, as shown in Fig. 2B. The SEM images also indicate that α-RuO_2 is possibly located on the nanotube walls. In contrast, for RuO_2^{TD}/TNA, the RuO_2 deposit with larger individual nanoparticles appears much thicker so that the underlying TNA is fully covered and blocked (Fig. 2 C), lowering the utilization of the RuO_2 to catalyze the CO_2RR. EDX analysis reveals that the atomic ratio of Ru:Ti is 3.77:36.86 for RuO_2^{CV}/TNA and 31.11:9.77 for RuO_2^{TD}/TNA, respectively. Since the two RuO_2 deposits are supported on the same TNA, the amount of Ru in the RuO_2^{CV}/TNA electrode is roughly 1/30 of that in the RuO_2^{TD}/TNA one. In other words, the electrochemical deposition facilitates the control of growing ultrathin RuO_2 layers over TNA, increasing significantly Ru mass utilization.

The GI-XRD (Fig. 2 D) result confirms the phase change before and after depositing and annealing RuO_2^{CV}/TNA. Before the deposition of RuO_2 (Fig .2 D (a)), only the peaks of the TNA substrate show up. After the first potential cycling deposition of RuO_2 (Fig. 2 D (b)), the peaks for the TNA substrate at 36° and 54° are weakened, nevertheless no RuO_2 signals can be detected, suggesting that the deposited RuO_2 is amorphous[29]. After being annealed at 450 ℃ for 2 h (Fig. 2 D (c)), the sample shows two peaks at 28° and 35°, featuring the transition from amorphous RuO_2 structure to polycrystalline RuO_2 structure. The second potential cycling deposition of α-RuO_2 takes place on this underlying substrate for better adhesiveness, the resulting sample is denoted as RuO_2^{CV}/TNA, which is used for following electrochemical measurements.

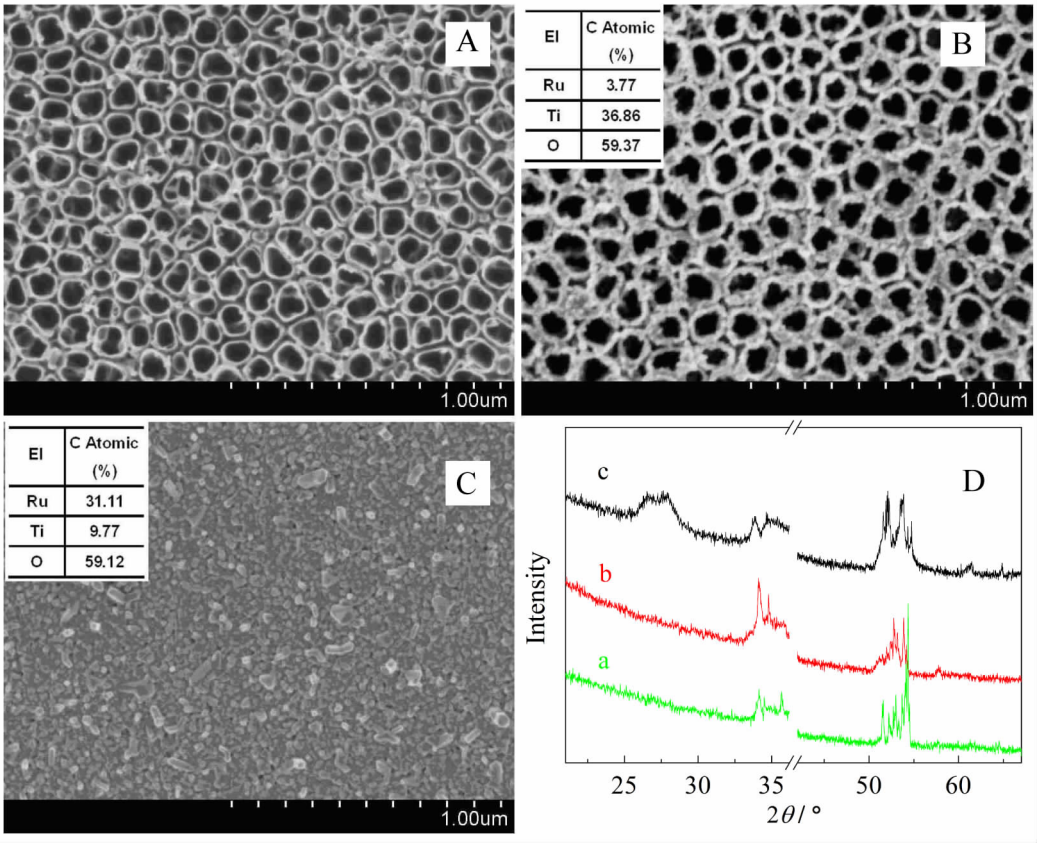

Fig. 2 FE-SEM images of as-prepared TNA (A), RuO_2^{CV} /TNA (B), RuO_2^{TD}/TNA (C), and GI-XRD (D) profiles for as-prepared TNA (a), α-RuO_2/TNA (b) and pc-RuO_2/TNA (c)

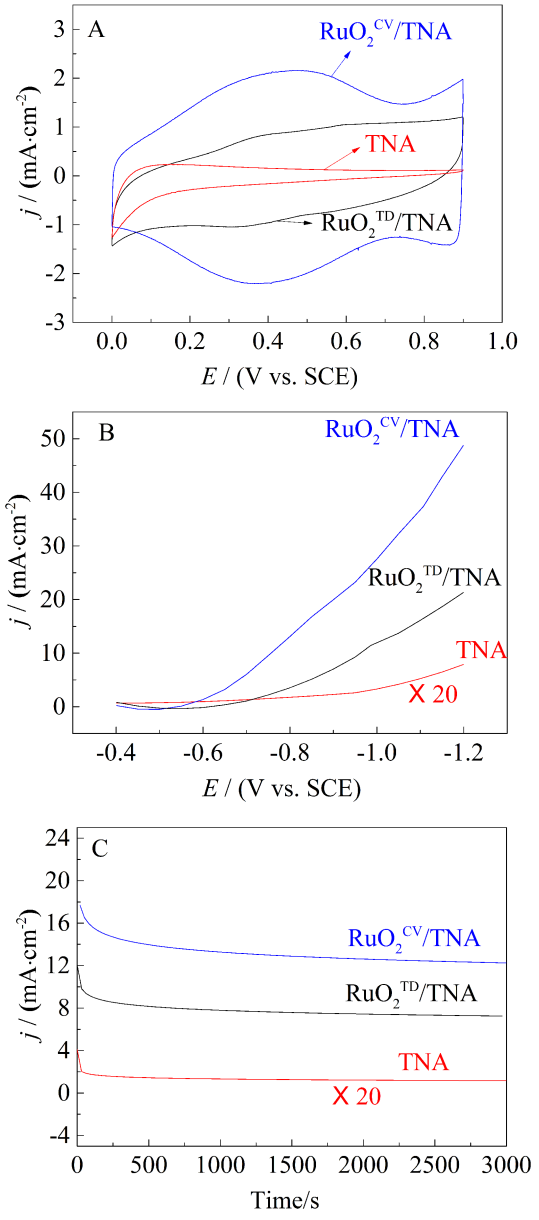

Fig.3 A. Cyclic voltammograms for RuO_2^{CV}/TNA, RuO_2^{TD}/TNA and TNA electrodes in (A) 0.5 mol·L^{-1} H_2SO_4 at scan rate of 50 mV·s^{-1}; B. Linear sweep voltammograms at 2 mV·s^{-1} and current vs. time plots for CO_2RR at -0.8 V (vs. SCE) in CO_2-saturated PBS (pH 7) for RuO_2^{CV}/TNA, RuO_2^{TD}/TNA and TNA electrodes(C).

The as-formed RuO_2^{CV}/TNA electrode was first electrochemically characterized in 0.5 mol·L^{-1} H_2SO_4, showing a fish-shaped voltammogram (Fig. 3 A), indicative of the formation of an α-RuO_2 outer layer[29-30], in contrast to an approximately square-shaped voltammogram for the polycrystalline RuO_2^{TD}/TNA electrode[16]. The electrocatalytic properties of the two electrodes were simply compared by recording linear sweep voltammograms (Fig. 3B) and chronoamperometric curves (Fig. 3 C), revealing that the RuO_2^{CV}/TNA electrode is superior to the RuO_2^{TD}/TNA one in terms of electrocatalytic performance. Specifically, the CO_2RR initialized at *ca.* -0.6 V (vs. SCE) on RuO_2^{CV}/TNA, or positively shifted by *ca.* 0.1 V, compared to that on RuO_2^{TD}/TNA, suggesting that α-RuO_2 may drive the CO_2RR at a smaller overpotential. Furthermore, a stablized reduction current of *ca.* 12 mA·cm^{-2} was detected on RuO_2^{CV}/TNA, which is *ca* 1.7 times of that on RuO_2^{TD}/TNA, consistent with a larger electrochemical active surface area inherent for the RuO_2^{CV}/TNA electrode. It should be pointed out the annealing treatment after the electrodeposition of an initial layer of α-RuO_2 benefits the subsequent electrodepositon of a second layer of α-RuO_2, leading to a larger electroactive surface area and an enhanced stability in electrocatalytic performance during CO_2RR. Table 1 lists the faradaic efficiencies (FEs) for formate, CH_4 and H_2 after polarizing the RuO_2^{TD}/TNA and RuO_2^{CV}/TNA electrodes at -0.8 V in CO_2-saturated PBS solution for 452 min, respectively. Although the two electrodes yield similar FEs, RuO_2^{CV}/TNA exhibits a significantly (1.7 times) higher current density with a much lower (*ca.* 1/30) Ru mass loading than RuO_2^{TD}/TNA.

We further examined the potential dependent selectivities of CO_2RR on the RuO_2^{CV}/TNA electrode in commonly used CO_2-saturated 0.1 mol·L^{-1} $KHCO_3$ electrolyte. The solution products and the gas products were analyzed by using NMR (see Fig. 4 A) and GC (Fig. 4 B and C), respectively. The spectral data were used to quantitatively calculate FEs and partial current densities for formate, CH_4 and CO as well as for H_2, at potentials varied from -0.8 to -1.2 V, see Fig. 5 A and B.

In comparison with the results listed in Tab.1, small amount of CO with FE up to 2.7% was additionally detected during CO_2RR on RuO_2^{CV}/TNA in 0.1 mol·L^{-1} $KHCO_3$ solution. It can be seen that the highest FE for formate, *ca.* 32 % occurs at -0.9 V vs. SCE, with a highest partial reduction current of *ca.*

Tab. 1 Faradaic efficiencies for CO_2RR on the RuO_2^{TD}/TNA and RuO_2^{CV}/TNA electrodes at -0.8 V (vs. SCE) in a PBS solution (pH 7).

Electrode	Total charge/C	Product faradaic efficiency/%			
		Formate	CH_4	H_2	CO
RuO_2^{TD}/TNA	31.58	30.98	1.05	32.58	Undetected
RuO_2^{CV}/TNA	45.05	29.24	1.59	34.35	Undetected

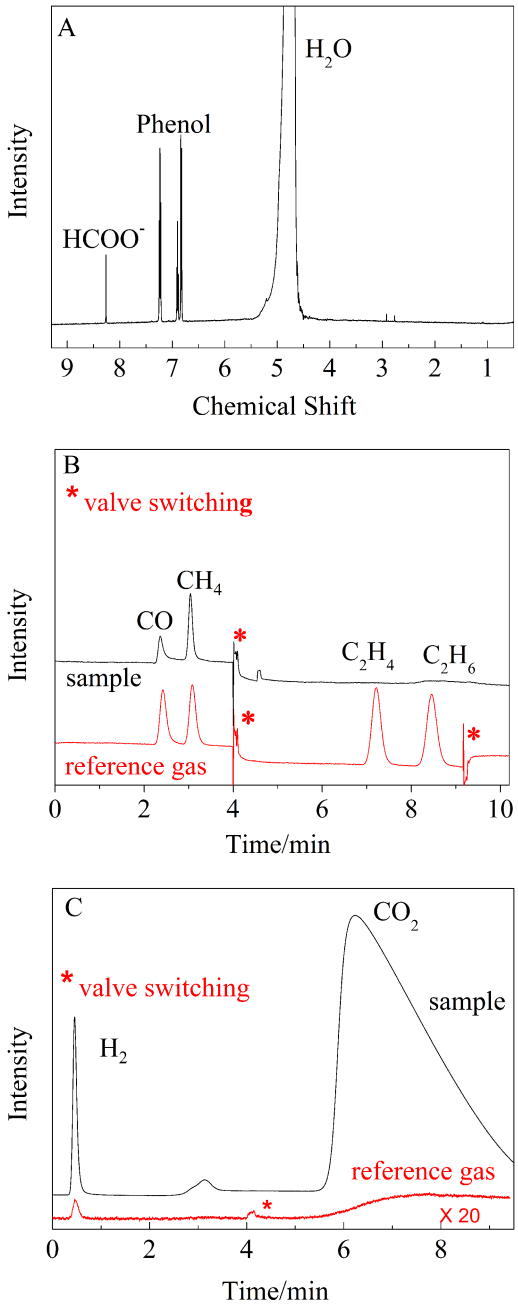

Fig. 4 A. ^1H NMR spectrum of the liquid products, B. GC traces from FID channels of the gas products and TCD channels of the gas products in CO_2-saturated 0.1 mol·L^{-1} $KHCO_3$ for 2 h (C).

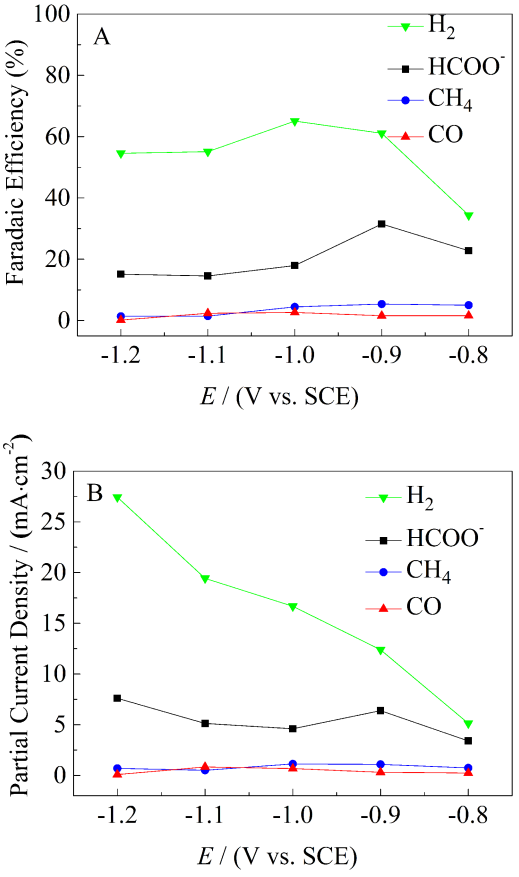

Fig. 5 Faradaic efficiencies (A) and partial current densities (B) for CO_2RR on the RuO_2^{CV}/TNA electrode at different potentials (vs. SCE) in CO_2-saturated 0.1 mol·L^{-1} $KHCO_3$ for 2 h

6.4 mA·cm^{-2}. Also notably, FE for CH_4 varies from 1.4 % to 5.5 %, specifically it is *ca.* 5.4 % at -0.8 V and 5.5% at -0.9 V, much higher than that listed in Tab.1. It also can be seen that H_2 production during CO_2RR contributes largely to the resulting reduction current. Further extension of the RuO_2^{CV}/TNA for other electrocatalytic applications is planned.

3 Conclusions

In this preliminary work, a controlled deposition

of α-RuO_2 layers on vertically oriented TNA on Ti is enabled through two-step potential cycling in a Ru(III) chloride precursor solution. The α-RuO_2 layers are well-dispersed on the walls of the TNA without damaging the nanotube structure, and the corresponding Ru loading decreases to be *ca.* 1/30 of that for polycrystalline RuO_2 layers on TNA formed through thermal decomposition of a Ru(III) precursor. The RuO_2^{CV}/TNA electrode displays an overall reduction current that is 1.7 times of that obtained on the RuO_2^{TD}/TNA one with an initial reduction potential positively shifted by 100 mV, despite that the two electrodes give the similar faradaic efficiencies for the reduction products including formate and CH_4 in a CO_2-saturated PBS solution of pH 7. CO_2RR on the RuO_2^{CV}/TNA electrode in CO_2-saturated 0.1 mol·L^{-1} $KHCO_3$ produces additional CO apart from formate and CH_4, showing that highest faradaic efficiencies for formate and CH_4 occurs at -0.9 V.

Acknowledgements:

This work is supported by the 973 Program (No. 2015CB932303) of MOST and NSFC (No. 21473039).

References:

[1] Zhang Z F, Xie E, Li W J, et al. Hydrogenation of carbon dioxide is promoted by a task-specific ionic liquid[J]. Angewandte Chemie International Edition, 2008, 47(6): 1127-1129.

[2] Barrosse-Antle L E, Compton R G. Reduction of carbon dioxide in 1-butyl-3-methylimidazolium acetate[J]. Chemical Communications, 2009, (25): 3744-3746.

[3] Woolerton T W, Sheard S, Reisner E, et al. Efficient and clean photoreduction of CO_2 to CO by enzyme-modified TiO_2 nanoparticles using visible light[J]. Journal of the American Chemical Society, 2010, 132(7): 2132-2133.

[4] Angamuthu R, Byers P, Lutz M, et al. Electrocatalytic CO_2 conversion to oxalate by a copper complex[J]. Science, 2010, 327(5963): 313-315.

[5] Begum A, Pickup P G. Electrocatalysis of CO_2 reduction by ruthenium benzothiazole and bithiazole complexes[J]. Electrochemistry Communications, 2007, 9(10): 2525-2528.

[6] Saha M S, Furuta T, Nishiki Y. Conversion of carbon dioxide to peroxycarbonate at boron-doped diamond electrode[J]. Electrochemistry Communications, 2004, 6(2): 201-204.

[7] Liu L J, Li Ying. Understanding the reaction mechanism of photocatalytic reduction of CO_2 with H_2O on TiO_2-based photocatalysts: A review[J]. Aerosol and Air Quality Research, 2014,14(2): 453-469

[8] Neatu S, Macia-Agullo J A, Garcia H. Solar light photocatalytic CO_2 reduction: General considerations and selected bench-mark photocatalysts[J]. International Journal of Molecular Sciences, 2014, 15(4): 5246-5262.

[9] Reske R, Duca M, Oezaslan M, et al. Controlling catalytic selectivities during CO_2 electroreduction on thin Cu metal overlayers[J]. The Journal of Physical Chemistry Letters, 2013, 4(15): 2410-2413.

[10] Zhang S, Kang P, Meyer T J. Nanostructured Tin catalysts for selective electrochemical reduction of carbon dioxide to formate[J]. Journal of the American Chemical Society, 2014, 136(5): 1734-7.

[11] Gao D F, Wang J, Wu H H, et al. pH effect on electrocatalytic reduction of CO_2 over Pd and Pt nanoparticles[J]. Electrochemistry Communications, 2015, 55, 1-5.

[12] Min X Q, Kanan M. Pd-catalyzed electrohydrogenation of carbon dioxide to formate: High mass activity at low overpotential and identification of the deactivation pathway[J]. Journal of American Chemical Sociaty, 2015, 137(14):4701-4708.

[13] Hori Y. Electrochemical CO_2 reduction on metal electrodes[M]. Modern Aspects of Electrochemistry, Springer: New York, 2008, 42, 89-189.

[14] Cheung K C, Guo P, So M H, et al. Electrocatalytic reduction of carbon dioxide by a polymeric film of rhenium tricarbonyl dipyridylamine[J]. Journal of Organometallic Chemistry, 2009, 694(17): 2842-2845.

[15] Yano J, Yamasaki S. Pulse-mode electrochemical reduction of carbon dioxide using copper and copper oxide electrodes for selective ethylene formation[J]. Journal of Applied Electrochemistry, 2008, 38(12): 1721-1726.

[16] Spataru N, Tokuhiro K, Terashima C, et al. Electrochemical reduction of carbon dioxide at ruthenium dioxide deposited on boron-doped diamond[J]. Journal of Applied Electrochemistry, 2003, 33(12): 1205-1210.

[17] Bandi A. Electrochemical reduction of carbon-dioxide on conductive metallic oxides[J]. Journal of the Electrochemical Society, 1990, 137(7): 2157-2160.

[18] Chaplin R P S, Wragg A A. Effects of process conditions and electrode material on reaction pathways for carbon dioxide electroreduction with particular reference to formate formation[J]. Journal of Applied Electrochemistry, 2003, 33(12): 1107-1123.

[19] Zhou S H, Eichhorn B W, Jackson G. PtCu core-shell and

alloy nanoparticles for NO reduction; Anomalous stability and reactivity[J]. Abstracts of Papers - American Chemical Society, 2005, 230: U2145-U2145.

[20] Bandi A, Kuhne H M. Electrochemical reduction of carbon-dioxide in water-analysis of reaction-mechanism on ruthenium-titanium-oxide[J]. Journal of the Electrochemical Society, 1992, 139(6): 1605-1610.

[21] Qu J P, Zhang X G, Wang Y G, et al. Electrochemical reduction of CO_2 on RuO_2/TiO_2 nanotubes composite modified Pt electrode[J]. Electrochimica Acta, 2005, 50 (16/17): 3576-3580.

[22] Popic J., AvramovIvic M L, Vukovic N B. Reduction of carbon dioxide on ruthenium oxide and modified ruthenium oxide electrodes in 0.5 M $NaHCO_3$[J]. Journal of Electroanalytical Chemistry, 1997, 421(1/2): 105-110.

[23] Qin Y H, Yang H H, Lv R L, et al. TiO_2 nanotube arrays supported Pd nanoparticles for ethanol electrooxidation in alkaline media[J]. Electrochimica Acta, 2013, 106, 372-377.

[24] Liu S Q, Chen A C, Coadsorption of horseradish peroxidase with thionine on TiO_2: Nanotubes for biosensing[J]. Langmuir, 2005, 21(18): 8409-8413.

[25] Yoo J, Lee K, Schmuki P. Dewetted Au films form a highly active photocatalytic system on TiO_2 nanotube-stumps[J]. Electrochemistry Communications, 2013, 34: 351-355.

[26] Uddin M T, Nicolas Y, Olivier C, et al. Preparation of RuO_2/TiO_2 mesoporous heterostructures and rationalization of their enhanced photocatalytic properties by band alignment investigations[J]. The Journal of Physical Chemistry C, 2013, 117(42): 22098-22110.

[27] Tian M, Wu G S, Chen A C. Unique electrochemical catalytic behavior of Pt nanoparticles deposited on TiO_2 nanotubes[J]. ACS Catalysis, 2012, 2(3): 425-432.

[28] Chen B, Hou J B, Lu K. Formation mechanism of TiO_2 nanotubes and their applications in photoelectrochemical water splitting and supercapacitors[J]. Langmuir, 2013, 29 (19): 5911-5919.

[29] Hu C C, Huang Y H. Cyclic voltammetric deposition of hydrous ruthenium oxide for electrochemical capacitors[J]. Journalof the Electrochemical Society, 1999, 146 (7): 2465-2471.

[30] Mo Y B, Cai W B, Dong J A, et al. *In situ* surface enhanced raman scattering of ruthenium dioxide films in acid electrolytes[J]. Electrochemical and Solid State Letters, 2001, 4(9): E37-E38.

在 TiO_2 纳米阵列上电沉积 RuO_2 用于 CO_2 电还原

蒋 宇, 张莉娜, 秦先贤, 蔡文斌*

(复旦大学化学系, 能源材料化学协同创新中心, 上海市分子催化与功能材料表面重点实验室, 上海 200433)

摘要: 传统上, RuO_2/TiO_2 复合电极制备是通过在 TiO_2/Ti 基体上多次涂覆含 Ru 前驱体溶液和随后热分解(TD)来实现的. 为克服上述方法中 Ru 用量大和利用率低之不足, 本工作主要基于循环伏安法(CV)在 TiO_2 纳米管阵列(TNA)上电沉积 RuO_2 制备 RuO_2^{CV}/TNA 复合电极. SEM、GIXRD 和 CV 结果表明, 电沉积的 RuO_2 为无定型结构, 所制备电极中的 Ru 用量约为传统的 RuO_2^{TD}/TNA 电极中 Ru 用量的 1/30. 尽管两电极催化 CO_2 还原产物的法拉第效率接近, 但是 RuO_2^{CV}/TNA 电极比 RuO_2^{TD}/TNA 电极展示了更高的还原电流, 较正的初始还原电位和更好的稳定性. 与磷酸盐缓冲溶液中电还原 CO_2 相比, RuO_2^{CV}/TNA 电极在 0.1 mol·L^{-1} $KHCO_3$ 中电还原 CO_2 除生成更高法拉第效率的甲酸根和甲烷外, 还检测到 CO 的生成.

关键词: CO_2 还原; 无定型 RuO_2; TiO_2 纳米阵列; 电沉积